Fire suppression efficiency of water mists containing organic solvents

Yusuke Koshiba [1, a, *], Yohei Yamamoto [2, a], Hideo Ohtani [3]

[1] Department of Materials Science and Chemical Engineering, Faculty of Engineering, Yokohama National University, 79-5 Tokiwadai, Hodogaya-ku, Yokohama 240-8501, Japan

[2] Graduate School of Environmental and Information Sciences, Yokohama National University, 79-7 Tokiwadai, Hodogaya-ku, Yokohama 240-8501, Japan

[3] Department of Safety Management, Faculty of Environmental and Information Sciences, Yokohama National University, 79-7 Tokiwadai, Hodogaya-ku, Yokohama 240-8501, Japan

a: These authors contributed equally to this work and should be considered as co-first authors.

Abstract

This paper investigates the fire-suppression ability of water mists containing various organic solvents—ethanol, 1-propanol, tetrahydrofuran, methyl acetate, and 1,2-dimethyoxyethane—which form minimum-boiling azeotropic mixtures with water. The key factors influencing the suppression efficiencies of the solvent-containing water mists were elucidated by measuring the evaporation rates,

flash points, extinguishing times, and spray properties (droplet-size distribution, spray mass-flux density, and droplet velocity) of the mists. Suppression trials indicated that (i) heptane pool fires can be extinguished by aqueous solutions of ethanol and 1-propanol at solvent concentrations of 1.0–20.0 vol%, but are not consistently extinguished by the other three solvents, and (ii) the extinguishing times of aqueous ethanol and 1-propanol (despite their high flammability) are significantly shorter than those of a wet chemical (i.e., conventional fire-extinguishing agent). In a stepwise regression analysis, the fire-suppression abilities of water mists containing ethanol and 1-propanol were positively related to the spray flux density, spray velocity, and flash point, enabling an estimation of the extinguishing times. A correlation analysis demonstrated that a faster evaporation rate improves the fire-suppression ability. The results confirmed that ethanol and 1-propanol are effective additives to fire-extinguishing water mists. The study findings provide useful insights into the development of new water-mist fire suppressants, potentially making a large contribution to the reduction of fire-related fatalities and economic losses in industries.

Keywords: Fire suppression; Water mist containing organic solvent; Fire-extinguishing agent; Firefighting; Additive to water; Extinguishing time

1. Introduction

In Japan in 2018, 206 accidental fires and 403 spills occurred in industrial facilities that store and handle flammable liquids, causing a property loss of ca. 29.1 hundred million yen. Thus, an effective agent that contains and extinguishes a developing Class B fire is required in the chemical and petrochemical industries.

Water mist is expected as a more environmentally friendly fire suppressant in industrial facilities than ozone-depleting halocarbons (e.g., Halons 1301, 1211, and 2402). The National Fire Protection Association (NFPA) defines water mist as a water spray with $D_{v0.99} < 1000$ μm, where $D_{v0.99}$ is the 99th percentile of the volumetric diameter of the water droplets (NFPA, 2009). Because of their low inertia, water droplets less than approximately 10 μm in diameter drift freely and behave like a gas (Adida et al., 2007), whereas water droplets with diameters larger than 15 μm will fall under gravity (Husted et al., 2009). Water mist suppresses fire by several processes: cooling of the fuel surface and flame zone, displacement of the oxidant, and attenuation of thermal radiation (Chen et al., 2019).

A water mist with small-droplet size is advantageous for several reasons. Smaller water droplets increase the surface area in a given volume of water, promoting evaporation and enhancing the suppression efficiency. Wang et al. (2016) computationally found that the extinguishing time decreases as the water droplet size decreases from 100 to 900 μm. In contrast to large-droplet sprinkler systems, small-droplet water mists generally prevent or minimize the collateral damage caused by inundation.

They also prevent the splattering of water and burning oil. However, these advantages are somewhat offset by pivotal disadvantages. The low momentum of small droplets reduces their ability to penetrate the fire plume, thereby reducing the suppression efficiency of the water mist. Furthermore, as indicated by Liang et al. (2015) and Cong and Liao (2009), water mist cannot produce sufficient water vapor to extinguish a flame. Hence, it cannot adequately contain and extinguish small, developing fires.

When required, the suppression ability of water mist can be improved by additives. Typical water-mist additives include surfactants (Zhou et al., 2006) and inorganic compounds (e.g., $KHCO_3$ and K_2CO_3) (Feng et al., 2016). Transition metal compounds such as ferrocene are also effective flame inhibitors (Koshiba et al., 2016; Koshiba et al., 2015a; Koshiba et al., 2015b). However, these additives pose health and environmental concerns. Takahashi et al. (2007) reported a case study of a patient who suffered cardiac arrest (hyperkalemia) after accidentally ingesting a wet-chemical fire extinguisher (K_2CO_3 aq.). The fire-extinguishing agents of firefighting equipment must be non-toxic and non-corrosive, even in critical applications (Du et al., 2019). Goto and Ito (2013) experimentally investigated whether water containing 0.1–5% ethanol can extinguish pool fires. They reported that ethanol addition reduced the extinguishing time of pure water by a factor of three. However, they assessed only the extinguishing ability of ethyl alcohol, with little attempt to articulate the dominant factors enhancing the suppression efficiency.

To fill these gaps, the present study aims to (i) experimentally investigate the fire-suppression

ability of water mists containing organic solvents, and (ii) elucidate the factors dominating the suppression efficiency of aqueous solutions of organic solvents. Five organic solvents with high evaporation rates and low surface tension were selected for the study: ethanol (C_2H_5OH, EtOH), 1-propanol (1-C_3H_7OH, 1-PrOH), tetrahydrofuran (C_4H_8O, THF), methyl acetate ($CH_3CO_2CH_3$, MeOAc), and 1,2-dimethoxyethane ($CH_3O(CH_2)_2OCH_3$, DME). Solvent–water systems based on the selected solvents form minimum-boiling azeotropes (Pereiro et al., 2012) with potentially enhanced evaporation rates. Ozturk and Erbil (2018) investigated the evaporation rates of ethanol–water droplets (2 μL) on fluoropolymer plates, and reported that ethanol-containing water evaporates more rapidly than pure water. A low surface tension is also beneficial, as it reduces the droplet diameter in most cases (Semião et al., 1996). Both of these characteristics may enhance the fire-suppression capability of additive-containing water mist over that of pure water mist. Moreover, unlike conventional fire-extinguishing agents, water mists containing organic solvents are free of surfactants, thereby lowering the safety and environmental risks. However, as these organic solvents are themselves flammable, their addition to pure water mists may reduce the fire-suppression ability of the mist.

The remainder of this paper is developed as follows. Section 2 describes the study materials, and Section 3 experimentally analyzes the extinguishing ability of organic solvents on pool fires. The evaporation rates of the sprayed sessile droplets are discussed in Section 4. The spray properties of the proposed solutions, namely, the droplet-size distribution, spray mass-flux density, and spray velocity,

are presented in Section 5. Section 6 examines the flash points of EtOH aq. and 1-PrOH aq. The key factors effecting the fire-suppression capability are presented in Section 7, and the fire-suppression mechanisms are discussed in Section 8. The paper concludes with Section 9.

2. Chemicals and materials

The five organic solvents (i.e., EtOH, 1-PrOH, THF, MeOAc, and DME) were of reagent grade with purities >99.5%. To avoid ionic contaminants, the water was freshly deionized to a conductivity below 1 μS cm^{-1}. Fires in the suppression trials were fueled by n-heptane (>99.0%). All organic solvents and fuels were used without further purification. A flat and smooth polytetrafluoroethylene (PTFE) plate was purchased from Nichias Corp. (Tokyo, Japan). The average roughness, R_a, and root mean square roughness, R_q, of the PTFE plate were 207 and 269 nm, respectively.

3. Suppression experiments

3.1 Experimental details

The experimental apparatus of the suppression trials is depicted in Fig. 1. With this apparatus, we

can simply evaluate and compare the suppression efficiency of the water mists with and without the organic solvents. In each trial, 80 mL of n-heptane was poured into an oil pan (82 mm in diameter) that was pre-cooled to room temperature. Once quasi-steady burning was reached (i.e., pre-burning), the nozzle placed 600 mm above the oil pan was activated. Owing to the difficulty of maintaining a constant spray mass-flux density (F_w), the volumetric flow rate ($\dot{Q}_{mist}$) in the suppression experiments was fixed at $\dot{Q}_{mist}$ = 250 mL min^{-1}. The spray cone angle θ, which depends on the concentration C_k of the organic solvent k, was originally set to ca. $\theta = 60°$.

To experimentally investigate the influences of the organic solvents and their concentrations on the extinguishing time, the average extinguishing times (t) and standard deviations (σ) were determined in twelve suppression trials of each solution. The average heat release rate of the fire source (HRR_f, 1.76 kW) was calculated by multiplying the fuel consumption rate (4.0×10^{-2} g s^{-1}) by the heat of combustion of the fuel (44 kJ g^{-1}).

3.2 Results obtained from the suppression trials

The variation of extinguishing time as a function of organic solvent concentration is shown in Fig. 2. Pure water mist was unable to extinguish the heptane fire, allowing a direct comparison of the suppression ability among the aqueous solutions. THF aq. (C_{THF} = 1.0 vol%) was able to extinguish

the pool fire (t_{THF} = 16.0 s); at THF concentrations above 5.0 vol%, it failed to do so, as shown in Fig. 2a. The same results were seen for MeOAc aq. (t_{MeOAc} = 12.2 s at C_{MeOAc} = 1.0 vol%). Similarly, DME aq. successfully extinguished the pool fire at C_{DME} = 1.0 vol% (t_{DME} = 4.0 s) and 5.0 vol% (t_{DME} = 5.2 s), but not at concentrations above 15.0 vol%.

Fig. 2b shows the relationship between the extinguishing time and the organic solvent concentration in the aqueous EtOH and 1-PrOH solutions. For reference, the extinguishing time of a conventional wet-chemical agent (an aqueous solution of 45 wt% potassium carbonate) is also shown (t = 12.9 s (Koshiba et al., 2015a)). Unlike the aqueous solutions of THF, MeOAc, and DME, the EtOH aq. and 1-PrOH aq. extinguished the pool fire over the whole concentration range tested in this study (i.e., 1.0–20.0 vol%). The extinguishing time of EtOH aq. approached a minimum value at C_{EtOH} = 7.0 vol%, whereas the 1-PrOH aq. exhibited a minimum at $C_{1\text{-}PrOH}$ = 3.0 vol%. This clearly indicates that these concentrations optimized the respective fire-suppressing abilities of these solutions.

4. Evaporation rates of sprayed sessile droplets

The fire-suppression capability of pure water mist is generally dominated by the spray characteristics, namely, the droplet size, spray velocity/momentum, and mist flux density (NFPA 750, 2009). The suppression abilities of the present solvent–water systems might also depend on the

flammability of the included organic solvents, and the evaporation rate of the sprayed mists. This section focuses on the evaporation rate.

4.1 Earlier related studies

Researchers have investigated the evaporation rates of pure water and aqueous ethanol solutions. For instance, Spedding et al. (1993) experimentally measured the evaporation rates of bulk aqueous solutions of ethanol at lower ethanol concentrations. Liu et al. (2008) monitored the evaporation rates of ethanol-containing water droplets (1 μL) on hydrophobized silicon plates, and Sefiane et al. (2008) reported that under 1,000 mbar pressure at an ambient temperature of 23 °C, methanol-containing water droplets have shorter lifetimes than pure water droplets on a smooth silicon wafer.

The microliter droplets mentioned in the earlier studies have millimeter-sized diameters. As discussed in Section 5, the droplet diameters in the present study were of micrometer-order. The evaporation rates of micrometer-sized droplets have been rarely reported in the literature (Erbil, 2012). Accordingly, the evaporation rates of the solvent–water droplets in the present study were determined by directly measuring the rates of mass change on a sprayed surface.

4.2 Experimental details

Fig. 3 illustrates the experimental apparatus for measuring the evaporation rates of the sprayed mists. Aqueous 0–20 vol% EtOH and 1-PrOH solutions were sprayed at a flow rate and spray angle of $\dot{Q}_{\mathrm{mist}}$ = 250 mL min^{-1} and θ = ca. 60°, respectively, similarly to the suppression trials described in Section 3.

Each mist was directly sprayed onto the flat, smooth PTFE plate (diameter: 90 mm, $\lambda_{\mathrm{PTFE}} = 2.5 \times 10^{-1}$ Wm^{-1}K^{-1}) placed on the measuring pan of the waterproof analytical balance (readability: 0.01 mg). The distance between the nozzle and PTFE plate was set to 600 mm. When a droplet is deposited on the substance, a new liquid–solid interface is formed. If the material has a high thermal conductivity, the evaporation rate of the droplet is affected by the heat conduction between the liquid and solid (i.e., the droplet–substance heat conduction). For this reason, water droplets evaporate more quickly from an aluminum plate than from a PTFE plate (David et al., 2007).

Evaporation experiments were conducted in a in a 0.7×1×1 m confined space under controlled conditions (i.e., an ambient temperature of 24.5 ± 1.5 °C and a relative humidity of 40 ± 4%). To protect the deposited droplets on the plate from surrounding disturbances, the top door of the draft shield was slid open while the other doors were closed, as depicted in Fig. 3. Each measurement was triplicated to confirm repeatability of the results.

When EtOH aq. and 1-PrOH aq. are sprayed onto a hydrophobic plate, some of the droplets may

coalesce into larger droplets. This phenomenon will decrease the evaporation rate if the spray density is high. To prevent coalescence in the present study, the mists were collected for only one second using a sheet with a slit.

4.3 Experimental results

The evaporation rate of a droplet is usually positively correlated with its surface area; specifically, the droplet volume to the power of two-thirds ($V^{2/3}$) decreases linearly with time (Liu et al., 2008). As noted earlier, the droplets sprayed on the PTFE plate were too small for accurate measurements of their contact angle and surface area. Thus, in this study, the evaporation rate of the sprayed droplets was determined by measuring the weight loss per unit time.

Crafton and Black (2004) reported that as water droplets evaporate, their contact angles gradually decrease, so their evaporation rate accelerates over time. To avoid this time-dependence of the evaporation rate, the mass changes of the sprayed droplets were measured only for a short time (one minute). The normalized mass of the droplets, M, is defined as:

$$M = \frac{m}{m_0}, \tag{1}$$

where m represents the mass of the droplets spayed onto the PTFE plate at a given time and m_0 is the initial mass of the sprayed droplets. The m_0 values of the solutions prepared with $C_{EtOH} = 0$ (i.e., pure water), 1.0, 5.0, 7.0, 10.0, 15.0, and 20.0 vol% were determined to be 6.10×10^1, 5.75×10^1, 5.95×10^1, 6.04×10^1, 5.99×10^1, 5.85×10^1, and 6.10×10^1 mg, respectively. Meanwhile, those of the 1-propanol–water droplets at $C_{1\text{-PrOH}} = 1.0$, 3.0, 5.0, 10.0, 15.0, and 20.0 vol% were 6.04×10^1, 6.24×10^1, 6.01×10^1, 5.91×10^1, 5.94×10^1, and 5.94×10^1 mg, respectively.

Fig. 4 plots the normalized droplet masses as functions of time. As expected, increasing the ethanol concentration enhanced the droplet evaporation rates, and the M values decreased linearly with time (Fig. 4a). The 1-propanol-containing water droplets exhibited a similar trend (Fig. 4b), in which the slope of the fitted straight line corresponded to the mass evaporation rate (M').

Table 1 lists the slopes of the lines depicted in Fig. 4. The coefficients of determination were extremely high (≥ 0.99), suggesting good linearity between the evaporation rates and times. Furthermore, the evaporation rate, M', significantly increased with volatile alcohol concentration in the solvent range of 0–20 vol%. The M' values of the pure water and 20-vol% ethanol–water droplet samples were determined to be -1.76×10^{-3} s^{-1} and -2.43×10^{-3} s^{-1}, respectively. The evaporation rate of the 20-vol% ethanol–water droplets was approximately 1.38 times that of the pure water droplets. These results reasonably corroborate the findings of Sefiane et al. (2003), who found that the lifetime on a PTFE plate is approximately 1.2 times smaller for a 25% ethanol–water droplet than for

a pure water droplet.

5. Spray characteristics

As noted earlier, the suppression efficiency is generally governed by the mist droplet size, spray pattern, spray flux density, and droplet momentum (NFPA 750, 2009). As such, this section discusses the effects of the following spray properties: the Sauter mean diameter of the mist droplet (D_{32}, Eq. (2)), the spray pattern, spray flux density, and spray velocity.

$$\boldsymbol{D_{32} = \sum_i n_i D_i^3 \Big/ \sum_i n_i D_i^2}, \qquad (\mathbf{2})$$

where n_i denotes the measured number of droplets with diameter D_i.

5.1 Experimental details

Typical methods for evaluating spray-droplet size include diffraction grating, photographic, freezing, immersion, and phase Doppler interferometry (PDI) techniques. The immersion technique uses an immiscible liquid to easily and directly observe the gathered droplets using a microscope

(Hurlburt and Hanratty, 2002). However, as water mists containing organic solvents are highly lipophilic, the diameters of the droplets captured in silicone oil dramatically decreased over a short time, and eventually vanished (Fig. 5). For this reason, the immersion method was deemed unsuitable for measuring the sizes of water droplets containing the lipophilic organic solvents in the present study.

The PDI technique permits in-situ and simultaneous measurement of droplet size distribution, spray mass flux density (F_w), and spray velocity (u_w), and was therefore adopted. The experimental apparatus used for evaluating the mist droplets, spray mass flux densities, and droplet velocities, including the PDI instrument (PDI TK-2, Artium Technologies Inc.), is presented in Fig. 6. The droplet-size range capability of the PDI TK-2 is approximately 1.5–1200 μm. The nozzle was placed 600 mm from the laser-beam intersection, which was aligned to the center of the spray cone. The solvent concentration range of the aqueous EtOH and 1-PrOH solutions was 0.0–20.0 vol%. The flow rate and spray angle were set to $\dot{Q}_{\mathrm{mist}}$ = 250 mL min^{-1} and θ = ca. 60° respectively, as done in the suppression trials and evaporation-rate measurements (Sections 3 and 4, respectively).

5.2 Resulting spray characteristics

The spray flux densities of the aqueous EtOH and 1-PrOH solutions are shown in Fig. 7a as a function of the solvent concentration C_k, varying from C_k = 0.0 to C_k = 20.0 vol%. The flux density

was found to strongly depend on the solvent concentration. The spray mass-flux density of the EtOH aq. and 1-PrOH aq. was maximized (F_w = 1.32 × 10^3 mg cm^{-2} min^{-1}) at C_{EtOH} = 7.0 vol% and $C_{1\text{-PrOH}}$ = 3.0 vol%, respectively. The solvent concentrations that maximized the spray mass-flux density were fully consistent with the results of Fig. 2.

The variations of the droplet diameter (D_{32}, $D_{v0.1}$ and $D_{v0.9}$) and spray velocity as a function of solvent concentration are shown in Fig. 7b and 7c, respectively, where $D_{v0.9}$ represents the diameters below which 90% of the volume of droplets are found. The D_{32} of pure water mist was 82.7 μm. In the solvent concentration range of 0–20 vol%, the D_{32} ranged from 82.7 μm to 118.5 μm in EtOH aq. (see Fig. 7b). The u_w of pure water mist was 1.83 m s^{-1}. As depicted in Fig. 7c, the u_w values ranged from 1.83 to 2.36 m s^{-1} in the solvent concentration range of 0–20 vol%. These results indicate that the droplet diameters and spray velocities remained relatively constant.

The D_{32}, $D_{v0.1}$ and $D_{v0.9}$ values of both the EtOH–water and 1-PrOH–water droplets were found to be <100 μm, ca. 100 μm, and <200 μm, respectively. The water mists containing 0–20.0 vol% ethanol and 1-propanol were therefore categorized as Class 1 in the NFPA classification system.

6. Flash points

The low flash points of ethanol and 1-propanol restrict their practical applicability as extinguishing

agents. As noted by Koshiba et al. (2018), in their investigation of fire-extinguishing agents containing flammable components, the suppression effects of an active substance in a suppressant must surpass the flammability of the flammable components. Thus, this section investigates the flammability of the EtOH aq. and 1-PrOH aq. by experimentally and computationally investigating the flash points of the bulk EtOH aq. and 1-PrOH aq. liquids.

6.1 Experimental details

To elucidate the relationship between the flash point and solvent concentration, the flash points of the aqueous EtOH solutions were experimentally determined at solvent concentrations ranging from 0 to 20.0 vol%. Experiments were performed using a Tag closed-cup tester (TAG-E, Yoshida Kagaku Kaisha Co., Ltd, see Fig. 8) following a standard method (JIS, 2006). When the barometric pressure differed from 101.3 kPa, the observed flash points (T_{fp}^{ob}) were corrected to the actual, T_{fp}, by Eq. (3) (JIS, 2006):

$$\boldsymbol{T_{fp} = T_{fp}^{ob} + 0.25(101.3 - P)}, \quad (3)$$

where P denotes the ambient barometric pressure.

6.2 Flash-point calculations

To date, several methods for semi-empirically and theoretically estimating the flash points of binary mixtures are available in the literature. The pioneering model of Affens and McLaren (1972) estimates the flash points of hydrocarbon solutions (e.g., *n*-octane–*n*-undecane) in air by applying Dalton's and Raoult's laws; however, their approach is restricted to ideal solutions.

Non-ideal solutions can be obtained by activity-coefficient models such as the Wilson, non-random two-liquid (NRTL), universal quasi-chemical (UNIQUAC), and universal quasi-chemical functional-group activity coefficients (UNIFAC) equations. The major drawback of the Wilson model is its inapplicability to mixtures with a miscibility gap (Repke and Wozny, 2002) or in liquid–liquid equilibrium. UNIQUAC and three-parameter NRTL models based on the concept of local composition have been widely used (Benedetto et al., 2018), as they apply to both liquid–liquid and liquid–vapor equilibria. Other prediction models include analytical solution of groups (ASOG) (Tochigi et al., 1980) equations based on group-contribution methods, and the COSMO-RS method (Reinisch and Klamt, 2015), which quantum-chemically calculates the molecular surface-charge density.

In the present study, the flash points of EtOH aq. and 1-PrOH aq. were calculated by the UNIQUAC and COSMO-RS (ver. C30) methods. The UNIQUAC equations (Eqs. (4)–(14)) compute

the combinatorial and residual parts of the activity coefficients (γ_C and γ_R, respectively) as follows:

$$\ln\boldsymbol{\gamma_i} = \ln\boldsymbol{\gamma_{i,C}} + \ln\boldsymbol{\gamma_{i,R}}, \tag{4}$$

with

$$\ln\boldsymbol{\gamma_{i,C}} = \ln\left(\frac{\boldsymbol{\phi_i}}{\boldsymbol{x_i}}\right) + \frac{\boldsymbol{z}}{\boldsymbol{2}}\boldsymbol{q_i}\ln\left(\frac{\boldsymbol{\Theta_i}}{\boldsymbol{\phi_i}}\right) - \boldsymbol{\phi_j}\left[\boldsymbol{l_i} - \left(\frac{\boldsymbol{r_i}}{\boldsymbol{r_j}}\right)\boldsymbol{l_j}\right], \tag{5}$$

$$\ln\boldsymbol{\gamma_{i,R}} = \boldsymbol{q_i}\left[-\ln\left(\boldsymbol{\Theta_i} + \boldsymbol{\Theta_j\tau_{ji}}\right) + \boldsymbol{\Theta_j}\left(\frac{\boldsymbol{\tau_{ji}}}{\boldsymbol{\Theta_i} + \boldsymbol{\Theta_j\tau_{ji}}} - \frac{\boldsymbol{\tau_{ij}}}{\boldsymbol{\Theta_j} + \boldsymbol{\Theta_i\tau_{ij}}}\right)\right], \tag{6}$$

with

$$\boldsymbol{\phi_i} = \boldsymbol{x_i r_i} \Big/ \sum_{\boldsymbol{k}} \boldsymbol{x_k r_k}, \tag{7}$$

$$\boldsymbol{\phi_j} = \boldsymbol{x_j r_j} \Big/ \sum_{\boldsymbol{k}} \boldsymbol{x_k r_k}, \tag{8}$$

$$\boldsymbol{\Theta_i} = \boldsymbol{x_i q_i} \Big/ \sum_{\boldsymbol{k}} \boldsymbol{x_k q_k}, \tag{9}$$

$$\boldsymbol{\Theta_j = x_j q_j / \sum_k x_k q_k}, \tag{10}$$

$$\boldsymbol{l_i = \frac{z}{2}(r_i - q_i) - (r_i - 1)}, \tag{11}$$

$$\boldsymbol{l_j = \frac{z}{2}(r_j - q_j) - (r_j - 1)}, \tag{12}$$

$$\boldsymbol{\tau_{ij} = \exp\left(\frac{u_{ij} - u_{jj}}{RT}\right), \text{and}} \tag{13}$$

$$\boldsymbol{\tau_{ji} = \exp\left(\frac{u_{ji} - u_{ii}}{RT}\right)}. \tag{14}$$

In these expressions, ϕ and x are the volume and mole fractions, respectively, z is the coordination number (usually 10), q is the UNIQUAC surface parameter, θ is the surface-area fraction, l and τ are UNIQUAC parameters, r is the UNIQUC volume parameter, u is the intermolecular interaction parameter, R is the gas constant, and T is the temperature.

The flash points of the pure components (i.e., ethanol and 1-propanol) are provided in Table 2. In the UNIQUAC model, the flash point of pure ethanol was assumed as the generally accepted literature value (T_{fp} = 13 °C). Because the flash point of pure 1-propanol varies in the literature, it was assumed as 15 °C: the minimum acceptable value from a fire-safety perspective.

The COSMO-RS calculations were run in the COSMO*thermo* program (v. C30) with BP-TZVP-C30-1401 parameterization. The flame temperature was set to 1573 K (Reinisch and Klamt, 2015).

6.3 *Results obtained from the flash-point experiments*

The observed flash points of the aqueous EtOH aq. as a function of the H_2O mole fraction in the solution, x_{H2O}, which varied from $x_{H2O} = 0$ (i.e., the pure organic solvent) to $x_{H2O} = 1.0$ (i.e., pure water), are presented in Fig. 9a. The flash point gradually increased with x_{H2O} before rising steeply at $x_{H2O} >$ ca. 0.9.

Fig. 9a also displays the flash-point curves predicted by the UNIQUAC and COSMO-RS models. Comparing the experimentally observed data (open circles) with the solid (UNIQUAC) and dashed (COSMO-RS) curves, one finds that the UNIQUAC model predicted the experimental points to an accuracy of ±1.8 °C. At $x_{H2O} = 0$, the flash point (28.5 °C) calculated by the COSMO-RS model was significantly higher than the experimentally observed flash point (15°C) (see Fig. 9b). Thus, the flash points (Fig. 9c and 9d) calculated by the UNIQUAC equations are assumed in the regression analysis of Section 7.

7. Factors influencing the suppression efficiency of EtOH and 1-PrOH aq.

In Sections 3–6, the evaporation rates, spray properties (droplet size, spray flux density, and spray velocity), and flammability of the organic solvents used were investigated. In a regression analysis, this section quanti qzfies the effects of these characteristics on the fire-suppression capability of the solvents.

7.1 Regression analysis procedures

The general equation of multiple linear regression is given by

$$\widehat{\boldsymbol{Y}} = \left(\sum_{\mathbf{k=1}} \boldsymbol{B}_{\mathbf{k}}\boldsymbol{X}_{\mathbf{k}}\right) + \boldsymbol{B}_{\mathbf{0}}, \qquad (\mathbf{15})$$

where the regression coefficients, B_k, and regression constant, B_0, must minimize the sum of the squared differences between the actual Y and estimated $\hat{Y}$ for dependent variables X_k (Cohen et al., 2003a).

In the present multiple regression analysis, the extinguishing time was the dependent variable, and the spray properties (i.e., spray mass-flux density, spray velocity, and Sauter mean diameter of the mist droplets), evaporation rate, and flash point were the independent variables. To select the best

discriminating variables, a stepwise algorithm, which makes a large contribution to the coefficient of determination (R^2), was adopted. R^2 represents an index of fit of a regression model.

7.2 Results of the multiple regression analysis

The following variables were selected in the multiple regression models: F_w, u_w, and T_{fp}. A stepwise regression analysis revealed that all three coefficients were negative, indicating a negative relationship between the extinguishing time and each independent variable. In other words, these three variables were correlated with the fire-suppression efficiency. The homoscedasticity of the data was confirmed using the Breusch–Pagan test ($\chi^2 = 0.93$, $df = 3$, $p = 0.82 > 0.05$ for EtOH aq.; $\chi^2 = 4.73$, $df = 3$, $p = 0.19 > 0.05$ for 1-PrOH aq.). The final multiple regression models are summarized in Tables 3 (EtOH aq.) and 4 (1-PrOH aq.) and the regression equations of the predicted extinguishing times t_p are given by

$$\boldsymbol{t_{p,EtOH/water} = -1.13 \times 10^{-1} F_w - 5.94 \times 10^{-2} u_w - 7.60 \times 10^{-5} T_{fp} + 3.53 \times 10^{-1}}, \quad (16)$$

$$\boldsymbol{t_{p,1-PrOH/water} = -7.39 \times 10^{-2} F_w - 1.56 \times 10^{-2} u_w - 2.10 \times 10^{-4} T_{fp} + 2.27 \times 10^{-1}}. \quad (17)$$

Although these equations were created under the experimental conditions, the final three-predictor models accounted for 91.8% and 83.2% of the variances in $t_{p,\ EtOH\ aq.}$ ($R^2 = 0.92$) and $t_{p,\ 1\text{-}PrOH\ aq.}$ ($R^2 = 0.83$), respectively, indicating good fits to the data.

The multicollinearity was checked by calculating the variance inflation factor (VIF): a commonly used index of multicollinearity. A VIF exceeding 10 indicates serious multicollinearity problems involving the corresponding independent variables (Cohen et al., 2003b). As seen in Tables 3 and 4, the VIF values ranged from 1.56 to 2.82, clearly indicating the unlikelihood of multicollinearity.

The standardized beta coefficients of the regression equations for the spray mass-flux density, spray velocity, and flash point of the aqueous EtOH solution were determined to be −0.82, −0.24, and −0.04, respectively, and those of the aqueous 1-PrOH solution were −0.79, −0.07, and −0.12, respectively. As expected, the extinguishing time was highly dependent on the spray flux density and moderately dependent on the flash point.

The spray flux density and flash point were negatively correlated with the extinguishing time. While maintaining a constant flow rate, decreasing the spray angle gradually enlarged the spray flux. As spray fluxes are positively correlated with the viscosity and surface tension of the solvents (Spraying Systems, 2003), solvents with high viscosity and surface tension are required for high spray fluxes with enhanced fire-suppression capability.

As noted previously, the spray velocity was correlated with the extinguishing time. Consistent with

these findings, Grant et al. (2000) reported that in the 50–500 μm range of droplet diameters, increasing the spray velocity increases the flame penetration distance prior to evaporation, thereby increasing the heat transfer rate.

7.3 Results of the correlation analysis

Contrary to expectations, the regression analysis with stepwise regression did not choose evaporation-rate variables for the EtOH aq. and 1-PrOH aq. This likely occurred because the evaporation rate was strongly correlated with the other independent variables (i.e., the spray mass-flux density, spray velocity, Sauter mean diameter of the mist droplet, and flash point; see Tables 5 and 6). The correlation coefficients between the extinguishing time and evaporation rate were 0.76 and 0.96 for the EtOH aq. and 1-PrOH aq., respectively, suggesting that the fire-suppression efficiency strongly depended on the evaporation rate and that a faster evaporation rate enhanced the fire-suppression capabilities, as initially expected.

8. Suppression mechanisms

Under three assumptions—independence of heat capacity on temperature, a uniform temperature

profile of the flame (Liu et al., 2007), and no heat loss from the oil pan—the heat release rate ($\dot{Q}_{\mathrm{gen}}$) and heat loss rate ($\dot{Q}_{\mathrm{loss}}$) were calculated by Eqs. (18) and (19), respectively:

$$\dot{Q}_{\mathrm{gen}} = HRR_{\mathrm{f}} + x\dot{m}_{\mathrm{soln}}\Delta H_{\mathrm{c\,soln}}, \#(18)$$

$$\dot{Q}_{\mathrm{loss}} = \dot{m}_{\mathrm{f}}H_{\mathrm{v\,f}} + \dot{m}_{\mathrm{f}}c_{\mathrm{p\,f}}(T_{\mathrm{F}} - T_{\mathrm{f}}) + \dot{m}_{\mathrm{entrain}}c_{\mathrm{p\,a}}(T_{\mathrm{F}} - T_{\mathrm{a}}) + x\dot{m}_{\mathrm{soln}}H_{\mathrm{v\,soln}} + x\dot{m}_{\mathrm{soln}}c_{\mathrm{p\,soln}}(T_{\mathrm{b\,soln}} - T_{\mathrm{soln}}) + x\dot{m}_{\mathrm{soln}}c_{\mathrm{p\,v,soln}}(T_{\mathrm{F}} - T_{\mathrm{b\,soln}}), \#(19)$$

where x is the flame-entry rate of the suspended water mist containing the organic solvent, $\dot{m}_{\mathrm{soln}}$ and $\Delta H_{\mathrm{c\ soln}}$ are the mass evaporation rate and combustion enthalpy of the solvent-containing mist, respectively, $\dot{m}_{\mathrm{f}}$ is the fuel consumption rate, and $\Delta H_{\mathrm{v\,f}}$ and $c_{\mathrm{p,\,f}}$ are the vaporization enthalpy and heat capacity of the fuel, respectively. T_{F}, $T_{\mathrm{f,}}$ and T_{a} are the temperatures of the flame, the fuel in the oil pan, and the air, respectively. $\dot{m}_{\mathrm{entrain}}$ and $c_{\mathrm{p,\,a}}$ are the flow rate and heat capacity of the entrained air, respectively, $H_{\mathrm{v\ soln}}$ is the vaporization enthalpy of the solvent-containing mist, $c_{\mathrm{p\ soln,}}$ and $T_{\mathrm{b,\ soln}}$ are the heat capacity and boiling point of the solution, respectively, T_{soln} is the temperature of the sprayed solvent-containing mist, and $c_{\mathrm{p\ v,\ soln}}$ is the heat capacity of the solvent-containing mist. Thus, the second term on the right-hand side of Eq. (18) computes the heat release rate of the solvent-containing mist, while the first, second, third, fourth, fifth, and sixth terms on the right-hand side of

Eq. (19) denote the heat absorption rate of the fuel evaporation, the sensible heat absorption rate of the fuel, the sensible heat absorption rate of the entrained air, the heat absorption rate of the mist evaporation, the sensible heat absorption rate of the solution vapor, and the sensible heat absorption rate of the solution vapor ($T_b \rightarrow T_F$), respectively. The flame is extinguished when its temperature T_F (determined by the balance of $\dot{Q}_{gen}$ and $\dot{Q}_{loss}$) reduces to the point at which combustion cannot be maintained.

As stated in Section 3.2, a heptane pool fire cannot be extinguished by pure water mist, but can be extinguished by solvent-containing mists, because the solvents promote evaporation of the solution. Consequently, the flame zone is effectively cooled and the oxidant is displaced; these processes eventually extinguish the fire. Obviously, the suppression efficiency will be enhanced by increasing the spray mass-flux density and the evaporation rate. The extinguishing capability can also be enhanced by increasing the spray velocity of droplets with constant mass, because droplets carrying a high momentum can penetrate the fire plume. In contrast, the flammability of the sprayed mists is negatively correlated with suppression efficiency. Our experimental results suggest that the suppressing efficiency transcends the detrimental flammability of solvent-containing water mists.

This work was limited to five organic solvents. To clarify and generalize the influence of independent variables on the extinguishing time, further research on other organic-solvent/water solutions is required. Despite this limitation, this work gained an intriguing, unexpected insight into

why aqueous solutions of organic solvents can extinguish fires with high efficacy. In particular, the proposed additives EtOH and 1-PrOH are minimally toxic and highly biodegradable (on the Sigma–Aldrich safety sheets, both compounds are classified as non-corrosive and readily biodegradable), and therefore offer distinct advantages over surfactants.

9. Conclusions

This study explored the fire-suppression abilities of water mists containing five organic solvents (ethanol, 1-propanol, tetrahydrofuran, methyl acetate, and 1,2-dimethoxyethane), and the key factors influencing their suppression efficiency. The explorations focused on various experimental parameters: the evaporation rate, parameters of the spray characteristics (i.e., droplet-size distribution, spray mass-flux density, and droplet velocity), and the flash point. The following six conclusions were drawn from the study:

1. In suppression trials, pure water mist was unable to extinguish the pool fire, thus allowing a comparison of the suppression efficiency among the aqueous solutions of the solvents. In the 1.0–20.0 vol% range of solvent-concentrations, the suppression trials clearly demonstrated that heptane pool fires were extinguished by water mists containing EtOH aq. and 1-PrOH aq., but

were not consistently extinguished by THF aq., MeOAc aq., and DME aq. The extinguishing time was minimized at EtOH aq. and 1-PrOH aq. concentrations of 7.0 vol% and 3.0 vol%, respectively.

2. The extinguishing times of 1.0–20.0 vol% EtOH aq. and 1-PrOH aq. were significantly shorter than that of a conventional fire-extinguishing agent (i.e., an aqueous solution of 45 wt% potassium carbonate).

3. In evaporation-rate measurements of the sprayed droplets, the evaporation rates of the micron-sized EtOH–water and 1-PrOH–water droplets increased as the volatile alcohol concentration in the solvent increased from 0.0 to 20.0 vol%.

4. The mass-flux densities of the EtOH aq. and 1-PrOH aq. were maximized at the solvent concentrations that minimized the extinguishing time (7.0 and 3.0 vol%, respectively).

5. The extinguishing times of water mists containing EtOH and 1-PrOH were successfully estimated in a stepwise regression analysis based on the spray flux densities, spray velocities, and flash points. The multiple regression analysis revealed a positive relationship between the suppression ability and these three independent variables.

6. The correlation analysis clarified that increasing the evaporation rate raises the fire-suppression efficiency.

In summary, this comprehensive assessment of fire-suppression ability of water mists containing organic solvents indicated the potential for ethanol and 1-propanol to be used as novel additives to fire-suppressing water mists, despite the high flammability of ethanol and 1-propanol. This finding is a major step toward the development of new and effective additives in water mists, and will potentially contribute to the reduction of fire-related fatalities and losses.

Acknowledgments

The immersion measurements were conducted at the Instrumental Analysis Center of Yokohama National University.

Conflict of interest

None of the authors have any conflicts of interest to declare.

Funding

This work was supported by JSPS KAKENHI Grant Number JP19H02387 to Y.K.

References

Adiga, K.C., Hatcher Jr., R.F., Sheinson, R.S., Williams, F.W., Ayers, S. 2007. A computational and experimental study of ultra fine water mist as a total flooding agent. Fire Saf. J. 42, 150–160. https://doi.org/10.1016/j.firesaf.2006.08.010.

Affens, W.A., McLaren, G.W., 1972. Flammability properties of hydrocarbon solutions in air. J. Chem. Eng. Data 17, 482–488.

Chen, X., Fan, A., Yuan, B., Sun, Y., Zhang, Y., Niu, Y., 2019. Renewable biomass gel reinforced core-shell dry water material as novel fire extinguishing agent. J. Loss Prev. Process Ind. 59, 14–22. https://doi.org/10.1016/j.jlp.2019.02.008.

Cohen, J., Cohen, P., West, S.G., Aiken, L.S., 2003a. Applied Multiple Regression/Correlation Analysis for the Behavioral Sciences. Routledge (Taylor & Francis Group), third ed., pp. 64–100, Croydon.

Cohen, J., Cohen, P., West, S.G., Aiken, L.S., 2003b. Applied Multiple Regression/Correlation Analysis for the Behavioral Sciences. Routledge (Taylor & Francis Group), third ed., pp. 422–430,

Croydon.

Cong, B., Liao, G., 2009. Experimental studies on water mist suppression of liquid fires with and without additives. J. Fire Sci. 27, 101–123. https://doi.org/10.1177/0734904108095339.

Crafton, E.F., Black, W.Z., 2004. Heat transfer and evaporation rates of small liquid droplets on heated horizontal surfaces. Int. J. Heat Mass Transf. 47, 1187–1200. https://doi.org/10.1016/j.ijheatmasstransfer.2003.09.006.

Crowl, D.A., Louvar, J.F., 2011. Chemical Process Safety: Fundamentals with Applications, Pearson Education, Inc, third ed., pp. 653–658, Boston.

David, S., Sefiane, K., Tadrist, L., 2007. Experimental investigation of the effect of thermal properties of the substrate in the wetting and evaporation of sessile drops. Colloid Surf. A Physicochem. Eng. Asp. 298, 108–114. https://doi.org/10.1016/j.colsurfa.2006.12.018.

Di Benedetto, A., Sanchirico, R., Di Sarli, V., 2018. Flash point of flammable binary mixtures: Synergistic behavior. J. Loss Prev. Process Ind. 52, 1–6. https://doi.org/10.1016/j.jlp.2018.01.005.

Du, D., Shen, X., Feng, L., Hua, M., Pan, X., 2019. Efficiency characterization of fire extinguishing compound superfine powder containing $Mg(OH)_2$. J. Loss Prev. Process Ind. 57, 73–80. https://doi.org/10.1016/j.jlp.2018.08.016.

Erbil, H.Y., 2012. Evaporation of pure liquid sessile and spherical suspended drops: A review, Adv. Colloid Interface Sci. 170, 67–86. https://doi.org/10.1016/j.cis.2011.12.006.

Feng, M.-H., Tao, J.-J., Qin, J., Fei, Q., 2016. Extinguishment of counter-flow diffusion flame by water mist derived from aqueous solutions containing chemical additives. J. Fire Sci. 34, 51–68. https://doi.org/10.1177/0734904115618220.

Goto, M., Ito, A., 2013. Improvement of extinguishment performance of water mist with addition of small amount of ethanol. Shoken Shuho 67, 160–165 (in Japanese).

Grant, G., Brenton, J., Drysdale, D., 2000. Fire suppression by water sprays. Prog. Ener. Combust. Sci. 26, 79–130. https://doi.org/10.1016/S0360-1285(99)00012-X.

Hurlburt, E.T., Hanratty, T.J., 2002. Measurement of drop size in horizontal annular flow with the immersion method. Exp. Fluids 32, 692–699. https://doi.org/10.1007/s00348-002-0425-8.

Husted, B.P., Petersson, P., Lund, I., Holmstedt, G., 2009. Comparison of PIV and PDA droplet velocity measurement techniques on two high-pressure water mist nozzles. Fire Saf. J. 44, 1030–1045. https://doi.org/10.1016/j.firesaf.2009.07.003.

JIS 2265-1, 2006. Determination of Flash Point−Part 1: Tag Closed Cup Method, Tokyo.

Koshiba, Y., Agata, S., Takahashi, T., Ohtani, H., 2015b. Direct comparison of the flame inhibition efficiency of transition metals using metallocenes. Fire Saf. J. 73, 48–54. https://doi.org/10.1016/j.firesaf.2015.03.003.

Koshiba, Y., Iida, K., Ohtani, H., 2015a. Fire extinguishing properties of novel ferrocene/surfynol 465 dispersions. Fire Saf. J. 72, 1–6. https://doi.org/10.1016/j.firesaf.2015.02.011.

Koshiba, Y., Okazaki, S., Ohtani, H., 2016. Experimental investigation of the fire extinguishing capability of ferrocene-containing water mist. Fire Saf. J. 83, 90–98.

https://doi.org/10.1016/j.firesaf.2016.05.006.

Koshiba, Y., Tomita, T., Ohtani, H., 2018. Oil-in-water microemulsion containing ferrocene: A new fire suppressant. Fire Saf. J. 98, 82–89. https://doi.org/10.1016/j.firesaf.2018.04.005.

Laza, T., Bereczky, Á., 2011. Basic fuel properties of rapeseed oil-higher alcohols blends. Fuel 90, 803–810. https://doi.org/10.1016/j.fuel.2010.09.015.

Liang, T.L., Liu, M., Liu, Z., Zhong, W., Xiao, X., Lo, S., 2015. A study of the probability distribution of pool fire extinguishing times using water mist. Process Saf. Environ. Prot. 93, 240–248. https://doi.org/10.1016/j.psep.2014.05.009.

Liu, C., Bonaccurso, E., Butt, H.-J., 2008. Evaporation of sessile water/ethanol drops in a controlled environment. Phys. Chem. Chem. Phys. 10, 7150–7157. 10.1039/B808258H.

Liu, Z., Kim, A.K., Carpenter, D., 2007. A study of portable water mist fire extinguishers used for extinguishment of multiple fire types. Fire Saf. J. 42, 25–42. https://doi.org/10.1016/j.firesaf.2006.06.008.

NFPA 750, 2009. Standard on water mist fire protection systems, 2010 ed., Quincy, MA.

Noorollahy, M., Moghadam, A.Z., Ghasrodashti, A.A., 2010. Calculation of mixture equilibrium binary interaction parameters using closed cup flash point measurements. Chem. Eng. Res. Des. 88, 81–86. https://doi.org/10.1016/j.cherd.2009.07.002.

Ozturk, T., Erbil, H.Y., 2018. Evaporation of water-ethanol binary sessile drop on fluoropolymer surfaces: Influence of relative humidity, Colloid Surf. A Physicochem. Eng. Asp. 553, 327–336. https://doi.org/10.1016/j.colsurfa.2018.05.076.

Pereiro, A.B., Araújo, J.M.M., Esperança, J.M.S.S., Marrucho, I.M., Rebelo, L.P.N., 2012. Ionic liquids in separations of azeotropic systems—A review, J. Chem. Thermodyn. 46, 2–28. https://doi.org/10.1016/j.jct.2011.05.026.

Reinisch, J., Klamt, A., 2015. Predicting flash points of pure compounds and mixtures with COSMO-RS. Ind. Eng. Chem. Res. 54, 12974–12980. 10.1021/acs.iecr.5b03083.

Repke, J.-U., Wozny, G., 2002. Experimental investigations of three-phase distillation in a packed column. Chem. Eng. Technol. 25, 513–519. https://doi.org/10.1002/1521-4125(200205)25:5<513::AID-CEAT513>3.0.CO;2-8.

Sefiane, K., David, S., Shanahan, M.E.R., 2008. Wetting and evaporation of binary mixture drops. J. Phys. Chem. B 112, 11317–11323. 10.1021/jp8030418.

Sefiane, K., Tadrist, L., Douglas, M., 2003. Experimental study of evaporating water–ethanol mixture sessile drop: Influence of concentration. Int. J. Heat Mass Transf. 46, 4527–4534. https://doi.org/10.1016/S0017-9310(03)00267-9.

Semião, V., Andrade, P., de Graça Carvalho, M., 1996. Spray characterization: numerical prediction of Sauter mean diameter and droplet size distribution. Fuel 75, 1707–1714. https://doi.org/10.1016/S0016-2361(96)00163-9.

SFPE, 2002. SFPE handbook of fire protection engineering (third ed.), in: Kanury A.M. (Ed.), Ignition of Liquid Fuels. Massachusetts, pp. 2-188–2-199.

Spedding, P.L., Grimshaw, J., O'Hare, K.D., 1993. Abnormal evaporation rate of ethanol from low concentration aqueous solutions. Langmuir 9, 1408–1413.

Spraying Systems Co. USA, 2013. Optimizing your spray system: A guide to maximizing spray performance and reducing operating costs. https://www.spray.com/literature_pdfs/TM410B_Optimizing_Your_Spray_System.pdf (accessed 10 June 2019).

Takahashi Y., Suzuki S., Katsumi A., Harada N., Moroe Y., Kaburagi T., Nakazawa K., 2007. A case of cardiac arrest due to poisoning by the contents of a fire extinguisher. Nihon Kyukyu Igakukai Zasshi 18, 208–215. https://doi.org/10.3893/jjaam.18.208.

Tochigi, K., Hiraga, M., Kojima, K., 1980. Prediction of liquid–liquid equilibria for ternary systems by the ASOG method. J. Chem. Eng. Jpn. 13, 159–162. https://doi.org/10.1252/jcej.13.159.

Valenzuela, E.M., Vázquez-Román, R., Patel, S., Mannan, M.S., 2011. Prediction models for the flash point of pure components. J. Loss Prev. Process Ind. 24, 753–757. https://doi.org/10.1016/j.jlp.2011.04.010.

Wang, Z., Wang, W., Wang, Q., 2016. Optimization of water mist droplet size by using CFD modeling for fire suppressions. J. Loss Prev. Process Ind. 44, 626–632. https://doi.org/10.1016/j.jlp.2016.04.010.

Zhou, X., Z., Guangxuan, L., Bo, C., 2006. Improvement of water mist's fire-extinguishing efficiency with MC additive. Fire Saf. J. 41, 39–45. https://doi.org/10.1016/j.firesaf.2005.08.004.

Nomenclature

Symbols

B	Regression coefficient
B_0	Regression constant
C_k	Concentration of organic solvent k (vol%)
c_p	Heat capacity (kJ g^{-1} K^{-1})
D	Droplet diameter (μm)
$D_{v0.1}$	Volumetric diameter 10^{th} percentile (μm)
$D_{v0.9}$	Volumetric diameter 90^{th} percentile (μm)
$D_{v0.99}$	Volumetric diameter 99^{th} percentile (μm)
D_{32}	Sauter mean diameter, SMD (μm)

df	Degree of freedom
F_w	Spray mass-flux density (mg cm^{-2} min^{-1})
ΔH_c	Enthalpy of combustion (kJ g^{-1})
ΔH_v	Enthalpy of vaporization (kJ g^{-1})
HRR_f	Heat release rate of the fire source (kW)
l	UNIQUAC parameter defined in Eqs. (11) and (12)
M	Normalized mass of droplets (dimensionless)
M'	Evaporation rate of droplets spayed onto the PTFE plate (s^{-1})
m	Mass of droplets sprayed onto the PTFE plate at a given time (mg)
m_0	Initial mass of droplets sprayed onto the PTFE plate (mg)
$\dot{m}_{\mathrm{entrain}}$	Flow rate of the entrained air (g s^{-1})
$\dot{m}_f$	Fuel consumption rate (g s^{-1})
$\dot{m}_{\mathrm{soln}}$	Mass evaporation rate of the solvent-containing mist (g s^{-1})
n	Number of droplets
P	Ambient barometric pressure (kPa)
p	Probability
$\dot{Q}_{\mathrm{gen}}$	Heat release rate (kW)
$\dot{Q}_{\mathrm{loss}}$	Heat loss rate (kW)

$\dot{Q}_{\mathrm{mist}}$	Volumetric flow rate (mL $\mathrm{min^{-1}}$)
q	UNIQUAC surface parameter
R	Gas constant (8.31 J $\mathrm{mol^{-1}\ K^{-1}}$); also represents the correlation coefficient
R_{a}	Average roughness (nm)
R_{q}	Root mean square roughness (nm)
R^2	Coefficient of determination (dimensionless)
r	UNIQUAC volume parameter
T	Temperature (K)
T_{fp}	Corrected flash point in Eq. (3) (°C)
$T_{\mathrm{fp}}^{\mathrm{ob}}$	Observed flash points (°C)
t	Average extinguishing time (s)
t_{p}	Predicted extinguishing time (s)
u	Intermolecular interaction parameter (J $\mathrm{mol^{-1}}$)
u_{w}	Spray velocity (m $\mathrm{s^{-1}}$)
V	Droplet volume ($\mathrm{m^3}$)
X	An independent variable in its original units
x	Mole fraction (dimensionless)
Y	A dependent variable

$\hat{Y}$	A regression-estimated dependent variable Y
z	Coordination number (= 10)

Greeks

β	Standardized regression coefficient
γ	Activity coefficient (dimensionless)
Θ	Surface-area fraction (dimensionless)
θ	Spray cone angle (°)
λ	Thermal conductivity (W m^{-1} K^{-1})
σ	Standard deviation of extinguishing times (s)
τ	UNIQUAC parameter defined in Eqs. (13) and (14)
ϕ	Volume fraction (dimensionless)
χ^2	Chi-squared value

Subscripts

a	Air
adj	Adjusted
C	Combinatorial part

F	Flame
f	fuel
R	Residual part
soln	Solution

Abbreviations

aq.	Aqueous solution
ASOG	Analytical solutions of groups
COSMO-RS	Conductor like screening model for real solvents
DME	1,2-Dimethoxyethane
EtOH	Ethanol
MeOAc	Methyl acetate
NFPA	National Fire Protection Association
NRTL	Non-random two-liquid
PDI	Phase Doppler interferometry
1-PrOH	1-Propanol
PTFE	Polytetrafluoroethylene
SFPE	Society of Fire Protection Engineers

THF	Tetrahydrofuran
UNIFAC	Universal quasi-chemical functional-group activity coefficients
UNIQUAC	Universal quasi-chemical
VIF	Variance inflation factor

Table captions

Table 1

Mass evaporation rates M', and the R^2 values of pure water, ethanol–water, and 1-propanol–water droplets.

Table 2

Flash points of pure ethanol and 1-propanol published in the literature.

Table 3

Coefficients and VIF values in the final multiple regression model of EtOH aq.

Table 4

Coefficients and VIF values in the final multiple regression model of 1-PrOH aq.

Table 5

Zero-order correlation matrix for EtOH aq.

Table 6

Zero-order correlation matrix for 1-PrOH aq.

Figure captions

Figure 1

Schematic of the experimental apparatus for the suppression trials; 1: nozzle, 2: valve, 3: metering pump, 4: tank, 5: aqueous solution of the organic solvent, 6: oil pan, and 7: *n*-heptane.

Figure 2

Extinguishing times as functions of the organic-solvent concentration. In (a), the pentagons, triangles, and lozenges represent the aqueous solutions of tetrahydrofuran, methyl acetate, and 1,2-dimethoxyethane, respectively. In (b), the circles and hexagons denote the aqueous solutions of ethanol

and 1-propanol, respectively. Error bars indicate the standard deviations. The dashed line represents the extinguishing time of a wet-chemical agent (Koshiba et al., 2015a). As described in the text, the aqueous solutions of THF, MeOAc, and DME were unable to extinguish the pool fire at concentrations of ≥ 5.0, ≥ 5.0, and ≥ 15.0 vol%, respectively. Pure water mist failed to extinguish the pool fire.

Figure 3

Schematic of the experimental apparatus for the spray tests; 1: nozzle, 2: valve, 3: metering pump, 4: tank, 5: aqueous solution of the organic solvent, 6: PTFE plate (diameter = 90 mm), 7: waterproof analytical balance, 8: top door, and 9: sliding sheet with a slit. The top door of the analytical balance was slid open.

Figure 4

Normalized masses *M* of sprayed (a) EtOH–water droplets and (b) 1-PrOH–water droplets as functions of time.

Figure 5

Micrographs of the 5.0-vol% EtOH–water droplets collected using the immersion method after (a) 0 s, (b) 135 s, (c) 270 s, and (d) 290 s.

Figure 6

Schematic of the experimental apparatus for measuring the mist droplets, spray fluxes, and droplet velocities of the water mists containing ethanol and 1-propanol; 1: nozzle, 2: valve, 3: metering pump, 4: tank, 5: aqueous solution of the organic solvent, 6: laser, 7: beam splitter, 8: transmitter lens, 9: receiver lens, 10: photodetector, 11: signal processor, and 12: personal computer.

Figure 7

(a) Spray mass-flux density, (b) D_{32}, $D_{v0.1}$, and $D_{v0.9}$, and (c) droplet velocity as functions of organic-solvent concentration. The circles and triangles represent EtOH aq. and 1-PrOH aq., respectively.

Figure 8

Photograph of the Tag closed-cup tester used in the flash-point experiments.

Figure 9

Flash points of (a) EtOH aq. and (b) 1-PrOH aq. versus H_2O mole fraction; (c) flash point of EtOH versus ethanol concentration; and (d) flash point of 1-PrOH versus 1-propanol concentration. The circles denote the experimental values, and the blue-dashed and red-solid curves were calculated by

the COSMO-RS and UNIQUAC methods, respectively.

Figure 1

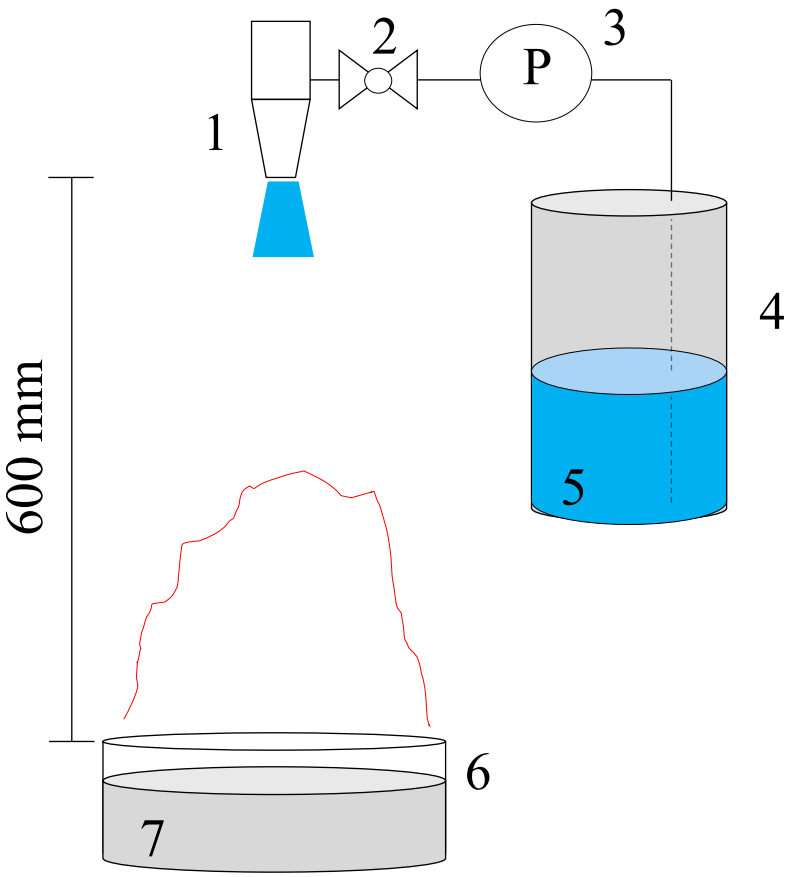

Figure 2

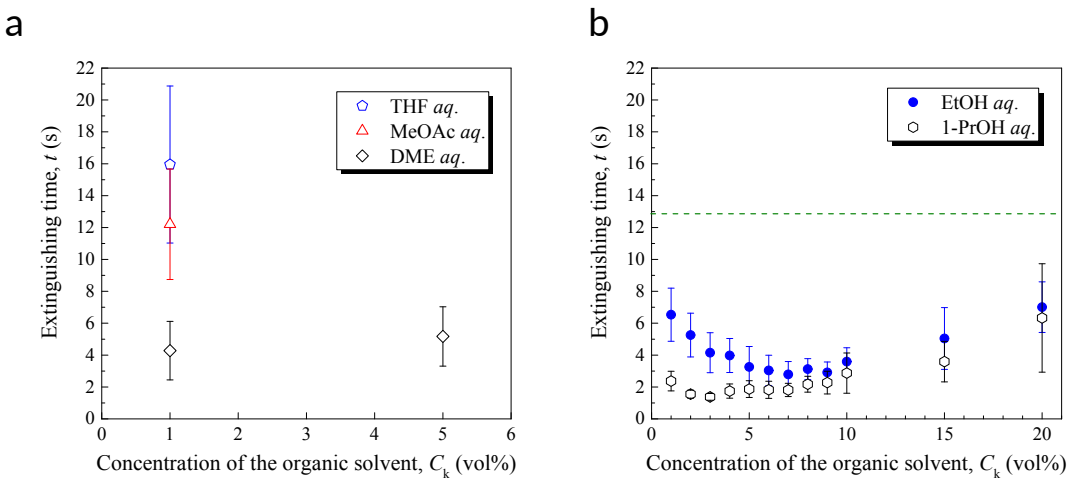
a
b
Extinguishing time, t (s)
Concentration of the organic solvent, C_k (vol%)
THF aq.
MeOAc aq.
DME aq.
EtOH aq.
1-PrOH aq.

Figure 3

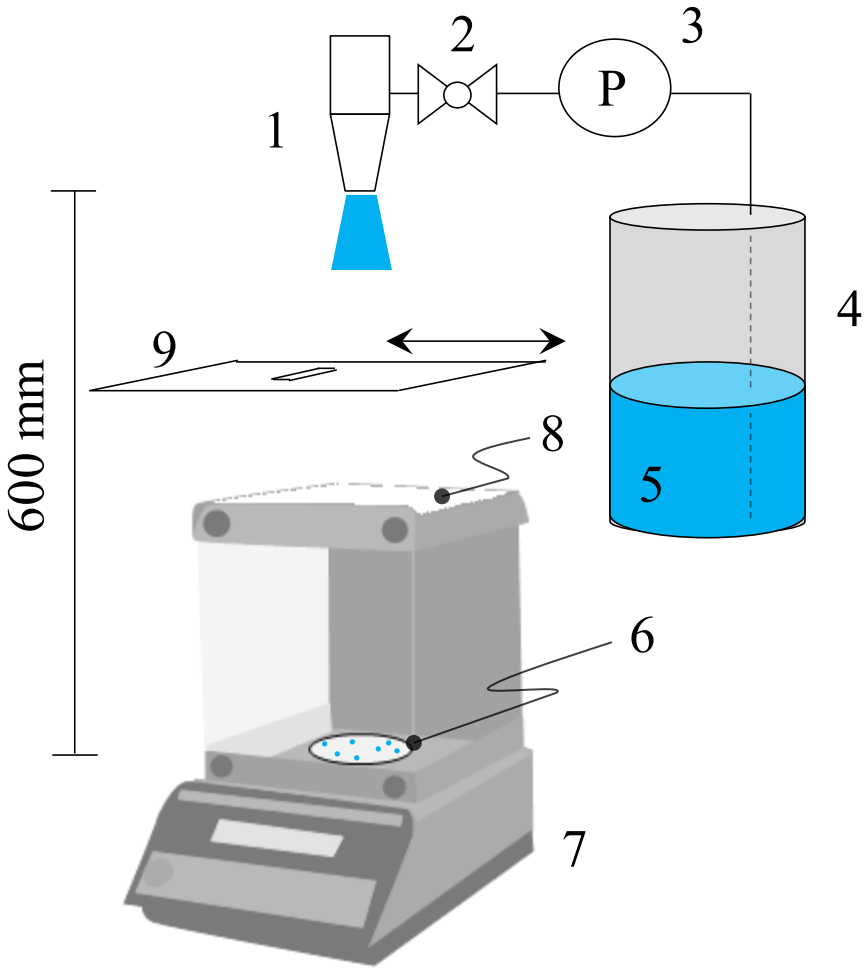

Figure 4

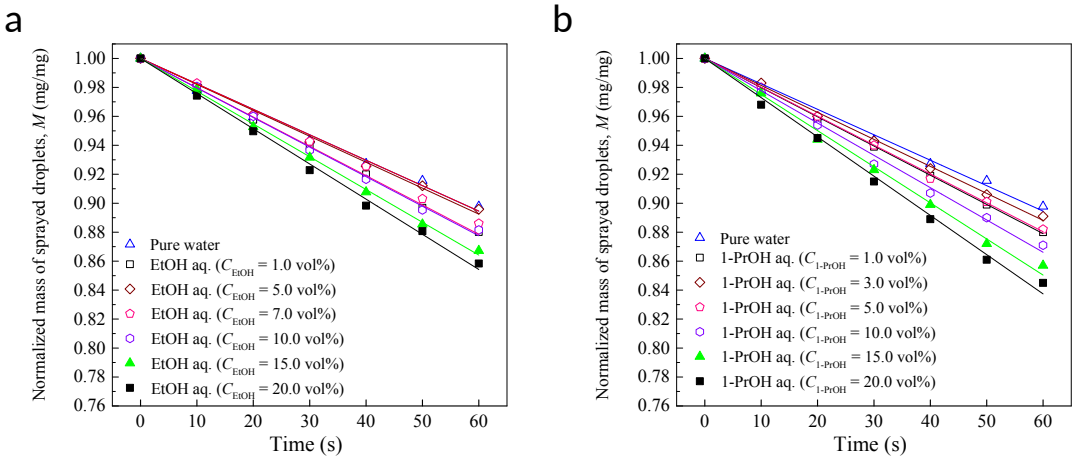
a
b
Normalized mass of sprayed droplets, M (mg/mg)
Time (s)
Pure water
EtOH aq. (C_EtOH = 1.0 vol%)
EtOH aq. (C_EtOH = 5.0 vol%)
EtOH aq. (C_EtOH = 7.0 vol%)
EtOH aq. (C_EtOH = 10.0 vol%)
EtOH aq. (C_EtOH = 15.0 vol%)
EtOH aq. (C_EtOH = 20.0 vol%)
1-PrOH aq. (C_1-PrOH = 1.0 vol%)
1-PrOH aq. (C_1-PrOH = 3.0 vol%)
1-PrOH aq. (C_1-PrOH = 5.0 vol%)
1-PrOH aq. (C_1-PrOH = 10.0 vol%)
1-PrOH aq. (C_1-PrOH = 15.0 vol%)
1-PrOH aq. (C_1-PrOH = 20.0 vol%)

Figure 5

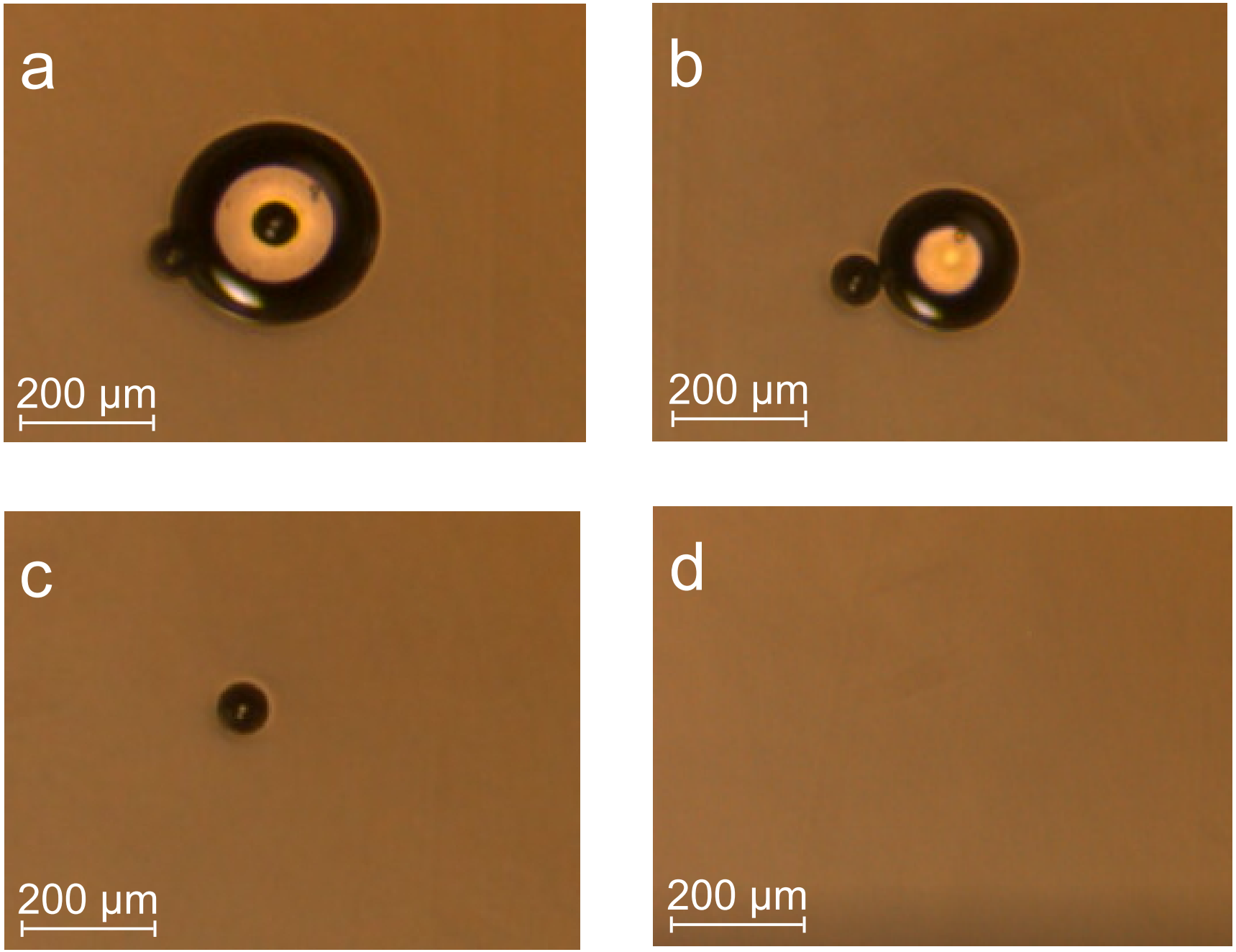

Figure 6

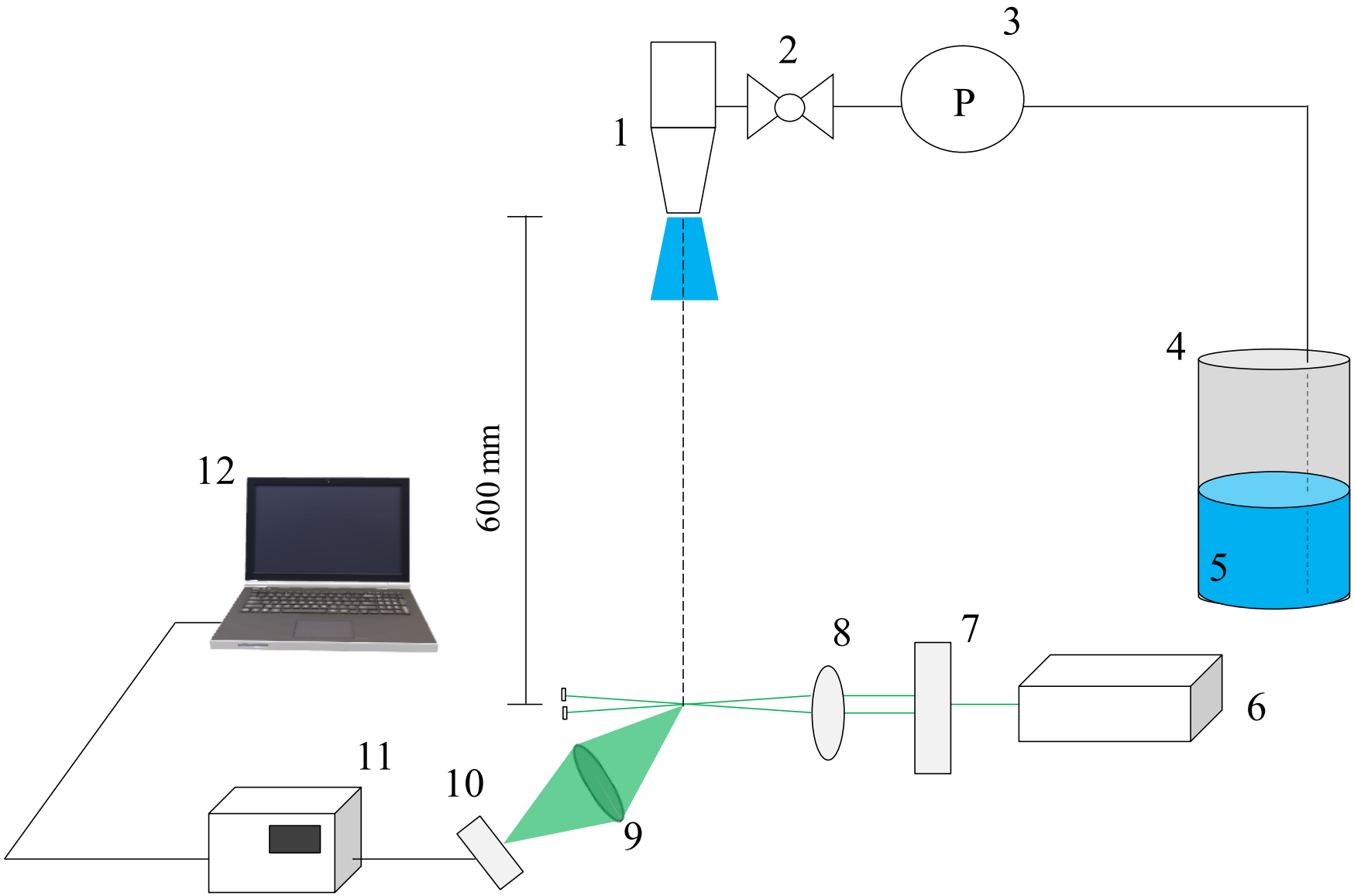

Figure 7

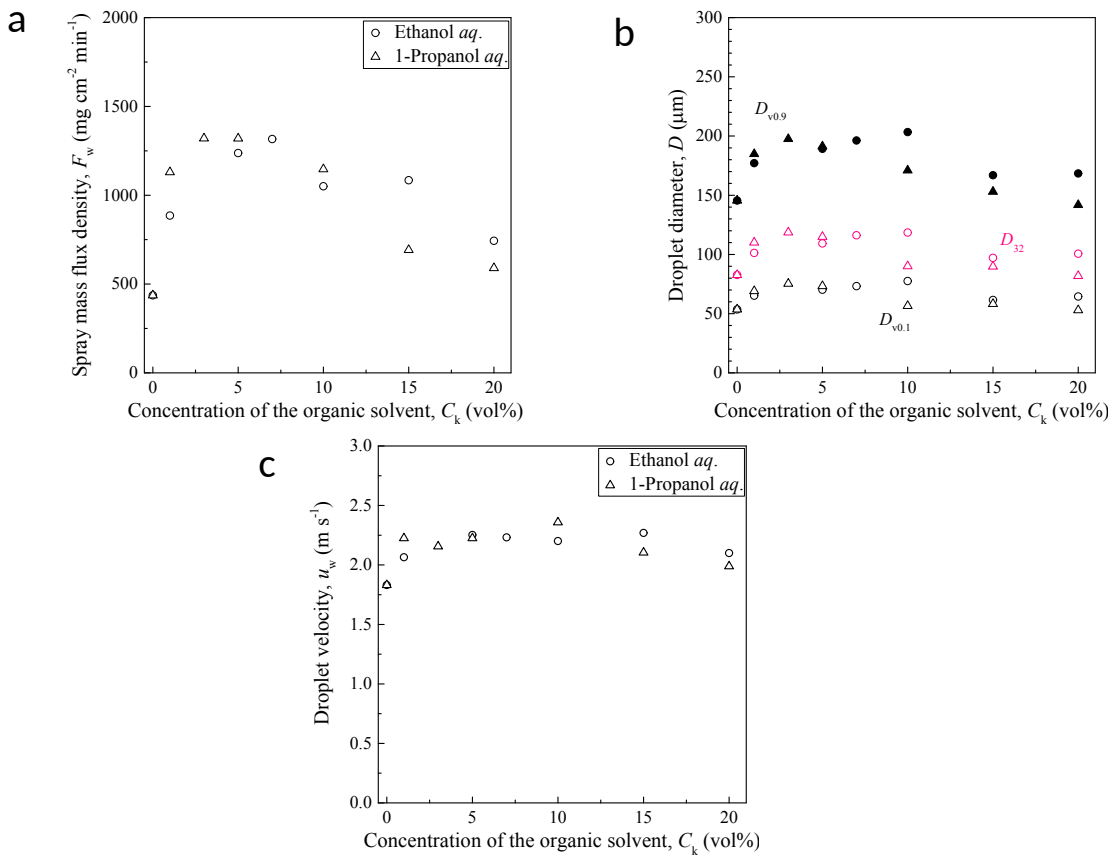
a
Spray mass flux density, F_w (mg cm^{-2} min^{-1})
Ethanol *aq*.
1-Propanol *aq*.
Concentration of the organic solvent, C_k (vol%)
b
Droplet diameter, D (μm)
$D_{v0.9}$
D_{32}
$D_{v0.1}$
Concentration of the organic solvent, C_k (vol%)
c
Droplet velocity, u_w (m s^{-1})
Ethanol *aq*.
1-Propanol *aq*.
Concentration of the organic solvent, C_k (vol%)

Figure 8

Figure 9

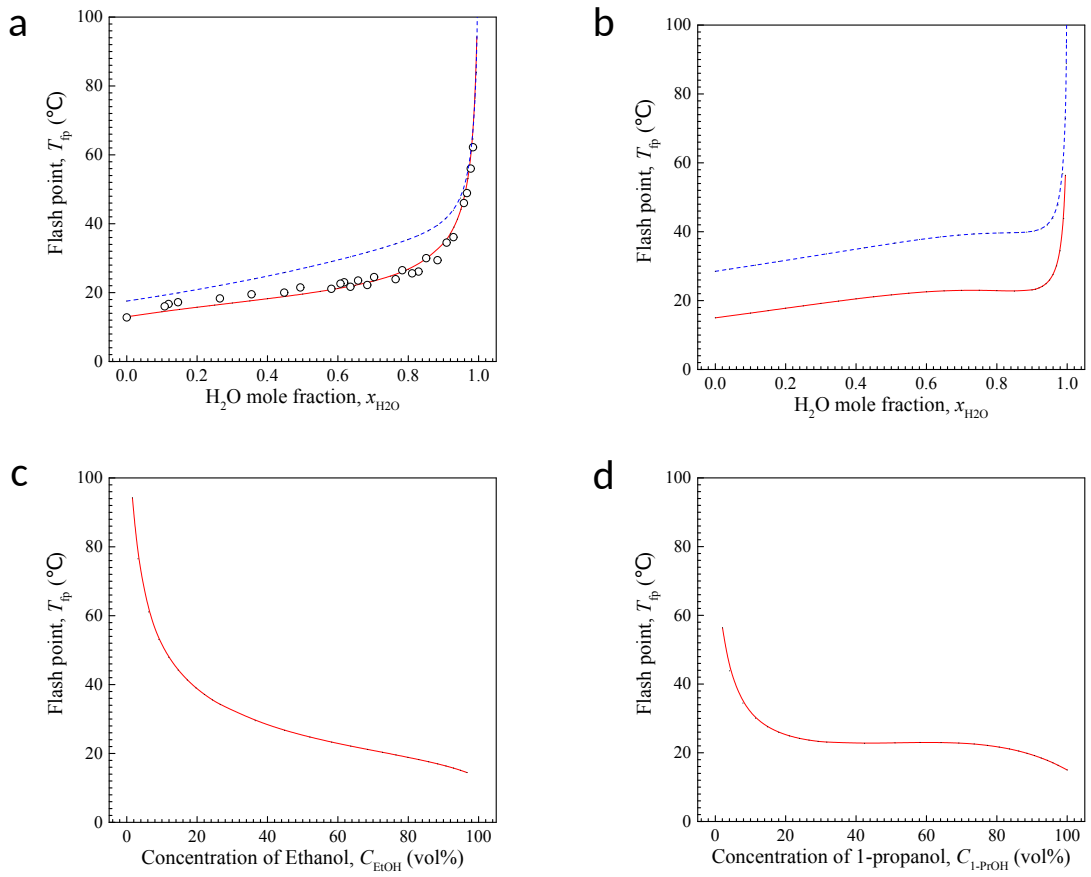
a
b
c
d
Flash point, T_{fp} (°C)
H_2O mole fraction, x_{H2O}
Concentration of Ethanol, C_{EtOH} (vol%)
Concentration of 1-propanol, $C_{1\text{-}PrOH}$ (vol%)

Table 1

Droplet sample	Slope of the line in Fig. 4 (i.e., *M'*) (s^{-1})	R^2
Pure water	-1.76×10^{-3}	1.00
1.0 vol% ethanol aq.	-2.02×10^{-3}	1.00
5.0 vol% ethanol aq.	-1.79×10^{-3}	0.99
7.0 vol% ethanol aq.	-1.90×10^{-3}	1.00
10.0 vol% ethanol aq.	-2.04×10^{-3}	1.00
15.0 vol% ethanol aq.	-2.26×10^{-3}	1.00
20.0 vol% ethanol aq.	-2.43×10^{-3}	1.00
1.0 vol% 1-propanol aq.	-2.02×10^{-3}	1.00
3.0 vol% 1-propanol aq.	-1.85×10^{-3}	1.00
5.0 vol% 1-propanol aq.	-1.99×10^{-3}	1.00
10.0 vol% 1-propanol aq.	-2.23×10^{-3}	0.99
15.0 vol% 1-propanol aq.	-2.49×10^{-3}	0.99
20.0 vol% 1-propanol aq.	-2.71×10^{-3}	0.99

Note: *M'* and R^2 represent the droplet evaporation rate and coefficient of determination of the line, respectively.

Table 2

Source	Flash point (°C) [a]	
	Ethanol	1-Propanol
Crowl and Louvar (2011)	13	15
SFPE (2002)	13	15
Valenzuela et al. (2011)	13	23
Laza and Bereczky (2011)	NA	15
Noorollahy et al. (2010)	13	21

a: Determined by the Tag closed-cup test.

Table 3

Independent variable	Unstd. coefficient		Std. coefficient β	VIF
	B	Std. error		
Constant	3.53×10^{-1}	2.65×10^{-1}		
F_w	-1.13×10^{-4}	3.66×10^{-5}	−0.82	1.69
u_w	-5.94×10^{-2}	6.71×10^{-2}	−0.24	1.84
T_{fp}	-7.60×10^{-5}	5.47×10^{-4}	−0.04	1.56

$R = 0.96$, $R^2 = 0.92$, $R_{adj}^2 = 0.79$.

Note: F_w, u_w, T_{fp}, B, and β denote the spray mass-flux density, spray velocity, flash point, regression coefficient in Eqs. (16) and (17), and standardized regression coefficient, respectively. VIF stands for the variance inflation factor.

Table 4

Independent variable	Unstd. coefficient		Std. coefficient β	VIF
	B	Std. error		
Constant	2.27×10^{-1}	2.79×10^{-1}		
F_w	-7.39×10^{-2}	4.54×10^{-2}	−0.79	2.82
u_w	-1.56×10^{-2}	9.85×10^{-2}	−0.07	2.08
T_{fp}	-2.10×10^{-4}	6.38×10^{-4}	−0.12	1.56

$R = 0.91$, $R^2 = 0.83$, $R_{adj}^2 = 0.58$.

Note: F_w, u_w, T_{fp}, B, and β denote the spray mass-flux density, spray velocity, flash point, regression coefficient in Eqs. (16) and (17), and the standardized regression coefficient, respectively. VIF stands for the variance inflation factor.

Table 5

	1	2	3	4	5
1. F_w					
2. u_w	0.45				
3. T_{fp}	0.25	−0.37			
4. M	−0.75	−0.34	−0.71		
5. D_{32}	0.58	0.43	0.18	−0.63	
6. t	−0.94	−0.60	−0.15	0.76	−0.79

Note: F_w, u_w, T_{fp}, M, D_{32}, and t represent the spray mass-flux density, spray velocity, flash point, normalized evaporation rate, Sauter mean diameter of the mist droplet, and extinguishing time, respectively.

Table 6

	1	2	3	4	5
1. F_w					
2. u_w	0.71				
3. T_{fp}	0.58	0.33			
4. M	−0.96	−0.60	−0.71		
5. D_{32}	0.86	0.33	0.73	−0.94	
6. t	−0.91	−0.67	−0.60	0.96	−0.87

Note: F_w, u_w, T_{fp}, M, D_{32}, and t represent the spray mass-flux density, spray velocity, flash point, normalized evaporation rate, Sauter mean diameter of the mist droplet, and extinguishing time, respectively.